Scanning probe lithography of self-assembled monolayers

Guohua Yang, Nabil A. Amro, Gang-yu Liu*
Department of Chemistry, University of California, Davis, CA, USA 95616

ABSTRACT

Systematic studies on scanning probe lithography (SPL) methodologies have been performed using self-assembled monolayers (SAMs) on Au as examples. The key to achieving high spatial precision is to keep the tip-surface interactions strong and local. Approaches include three atomic force microscopy (AFM) based methods, nanoshaving, nanografting, and nanopen reader and writer (NPRW), which rely on the local force, and two scanning tunneling microscopy (STM) based techniques, field-induced desorption and electron-induced desorption, which use electric field and tunneling electrons, respectively, for nanofabrication. The principle of these procedures, the critical steps in controlling local tip-surface interactions, and nanofabrication media will be discussed. The advantages of SPL will be illustrated through various examples of production and modification of SAM nanopatterns.

Keyword: scanning tunneling microscopy, atomic force microscopy, scanning probe lithography, nanofabrication, thiol, self-assembled monolayers

1. INTRODUCTION

Micro- and nano-fabrication of self-assembled monolayers (SAMs) on metal surfaces have attracted much attention in recent years, motivated by SAM's potential applications in molecular electronics,[1,2] micro and nanoelectromechanical systems (MEMS and NEMS),[3-5] chemical and biosensors,[6-9] and in the control of biomolecular adhesion on surfaces.[10-13] Micrometer-sized patterns have been fabricated within SAMs using microlithographic techniques, such as photolithography,[14,15] microcontact printing,[16,17] microwriting,[18,19] and micromachining.[19] Argon ion or electron beam lithography can produce smaller patterns (down to tens of nanometers) but require a high-vacuum environment.[20,21] Another approach to produce nanometer-sized structures of SAMs is the coadsorption of two or more adsorbates. However, with this approach, it is difficult to precisely control the size and distribution of these nanodomains because the structure is determined by the interplay of the kinetics and thermodynamics of the self-assembly process.[22-24]

Creating nanopatterns of SAMs with molecular precision requires new fabrication strategies. Scanning probe microscopy (SPM) techniques, such as scanning tunneling microscopy (STM)[25] and atomic force microscopy (AFM),[26] are well-known for their ability to visualize surfaces of materials with atomic level spatial resolution. Taking advantage of the sharpness of the tips, and strong and localized tip-surface interactions, SPM has also been used to manipulate atoms on metal surfaces and to fabricate nanopatterns of metal and semiconductor surfaces.[27-32]These successful examples catalyze an emerging field of scanning probe lithography (SPL). Recent progress in SPL of various materials has been discussed in several reviews.[33,34] Complementary to those studies, our research interests focus on SPL of SAMs. [35]

Despite the structural complexity of SAMs, molecular resolution images have been obtained using both AFM[36,37] and STM.[38-40] The fact that molecules within SAMs can be resolved indicates that the tip-SAM interaction in AFM imaging and the tunneling electrons in STM imaging are localized to molecular dimensions. Therefore, in principle, by enhancing these local interactions, such as force, density of tunneling electrons, and electrical field strength, chemical bonds can be broken selectively. The detailed methodology in controlling these local interactions is the key to obtaining sharp patterns with high spatial precision. Various approaches of controlling the local interactions have been reported. These methods include AFM-based lithography such as tip-catalyzed surface reactions,[41] dip-pen nanolithography,[42] and STM-based lithography such as tip-assisted electrochemical etching and field-induced desorption.[43]

In this study, we focus on our recent and systematic efforts in developing generic SPL-based methodologies to produce nanopatterns of SAMs. We first discuss the principle of our SPL procedures. The critical steps in controlling local tip-surface interactions will then be addressed. Media of SPL will also be discussed. The advantages of our approach will be illustrated through various examples of production and modification of SAM nanopatterns.

* liu@chem.ucdavis.edu; phone 1 530 754-9678; fax 1 530 752-8995

Proceedings of SPIE Vol. 5220 Nanofabrication Technologies, edited by Elizabeth A. Dobisz (SPIE, Bellingham, WA, 2003) · 0277-786X/03/$15.00

2. METHODOLOGY

2.1 Preparation of SAMs

Commercially available n-alkanethiols ($HS(CH_2)_nCH_3$, abbreviated as C_nSH): hexanethiol, octanethiol, decanethiol, dodecanethiol, octadecanethiol, 11-mercapto-undecanol ($HS(CH_2)_{11}OH$, abbreviated as $C_{11}OH$), 2-mercapto-propanoic acid ($HS(CH_2)_2COOH$, abbreviated as C_2COOH) and solvents of ethanol and sec-butanol were obtained from Aldrich and used as received.

Gold (Alfa Aesar, 99.99%) was deposited onto freshly cleaved mica substrates (Mica New York Corp., clear ruby muscovite) in a high vacuum evaporator (Denton Vacuum Inc., model DV502-A) at 6×10^{-7} Torr. Before deposition, the mica was preheated to 350 °C to enhance the formation of terraced Au(111) domains. The typical evaporation rate was 3 Å/s, and the thickness of the gold films ranged from 150 to 200 nm. The mica temperature was maintained at 350 °C for 15 min after deposition for annealing. This method produced samples with flat Au(111) terraces as large as 300×300 nm^2 according to our STM and AFM measurements.[44] These films were either used directly to prepare self-assembled monolayers or were fixed to a glass slide with an epoxy (EPO-TEK 377, Epoxy Tech.). These latter samples were separated at the gold-mica interface by peeling immediately before immersion in a thiol solution. This procedure produced gold substrates with flat surface terraces due to the templating effect of the atomically flat mica surface. AFM images revealed that the surfaces of these gold films had a mean roughness of ~5 Å over areas as large as several square micrometers.

Self-assembled monolayers (SAMs) were formed by soaking gold thin films (immediately after vacuum deposition or peeling) in dilute (0.01-1 mM) thiol solutions. Each gold substrate remained in a thiol solution for 1-7 days at room temperature to ensure the formation of mature monolayers with high coverage and a low density of defects.

2.2 Scanning tunneling microcopy

The UHV STM employed for our investigations has a base pressure of 2×10^{-10} torr. A variable temperature sample stage is available for thermal stability studies. The UHV system has a rapid-entry load-lock for sample and tip exchanges. The chamber is also equipped with a quadrupole mass spectrometer, an ion gun, and a sample/tip storage manipulator.

All STM images were acquired in a high-impedance, constant current mode. Typical imaging conditions for different thiol SAMs are bias voltages $V = \pm 0.5$ to ± 2.0 V, and tunneling current I = 1 to 100 pA. The STM tips used for these studies are tungsten wires cut under ambient condition, then electrochemically etched. A homemade electrochemical potentiostat was used to automatically monitor and stop the etching process when the current dropped below the setpoint. Typically, tips were etched at 2.1 V, in a 3M KOH solution. STM piezoelectric scanners were calibrated laterally with graphite(0001) and Au(111), and vertically using the height of Au(111) steps (2.35 Å). Calibrations were further verified by the periodicity of decanethiol SAMs on Au(111).

The relative tip-sample separation (Z) was determined from current-distance (I-Z) measurements. The zero separation is defined as tip-methyl contact, which can be identified easily as I-Z curves begin to change their slopes. The actual separation can be calculated from the approaching distance from the initial position to the contact point. Penetration distance is extracted from the approaching distance from the contact position to the final position. I-V measurements were acquired according to the following systematic steps. First, alkanethiol SAMs on Au(111) were imaged at a bias voltage of 1 V and a tunneling current of 5-30 pA, to reveal domains containing the $c(4\sqrt{3}\times 2\sqrt{3})R30^\circ$ superlattice. The STM tip was then parked at a designated location, where systematic I-V measurements could be acquired, above a thiol molecule within an ordered domain. We emphasize that all of the I-V curves shown in this article were acquired when the tip was in contact with the surface of the SAMs. The same area was imaged again after I-V measurements.

2.3 Atomic force microcopy

The atomic force microscope utilized a home-constructed, deflection-type scanning head that exhibits high mechanical stability. Samples were mounted inside a cell to allow imaging in a liquid environment while injecting or withdrawing solutions. Solvent was added to the cell as needed to compensate for its evaporation during the experiment. The scanner was controlled by an STM1000 electronics controller (RHK Technology, Inc.). Sharpened Si_3N_4 microlevers (Veeco Instruments) with a force constant of 0.1 N/m were used for AFM imaging and fabrication. Images were acquired in 2-butanol, which is an effective solvent for thiols and a good imaging medium, to avoid capillary interactions.

3. RESULTS AND DISCUSSION

3.1 STM-based lithography

The procedures of our STM-based lithography are illustrated in Figure 1. In STM-based lithography, the electric field and tunneling electrons are used to achieve nanofabrication of SAMs. As shown in Figure 1, STM images are acquired under low voltage and tunneling current, for example, 1.0 V and 20 pA for decanethiol SAMs with molecular level structural characterization. In field-induced desorption (Figure 1A), at a constant current in the pA range, increasing the bias voltage results in an increase in the electric field applied between the tip and the surface. The breakdown threshold voltage of SAMs is determined from current-voltage (I-V) measurements. The structural integrity of SAMs under the tip are monitored in situ by acquiring high-resolution images before and after nanofabrication. In current-induced desorption (Figure 1B), the tunneling current is slowly increased while the bias voltage is maintained constant. As the tunneling current is increased beyond the fabrication threshold, desorption of adsorbate molecules occurs (bottom panels in Figure 1B). The resulting patterns can then be imaged at a reduced current.

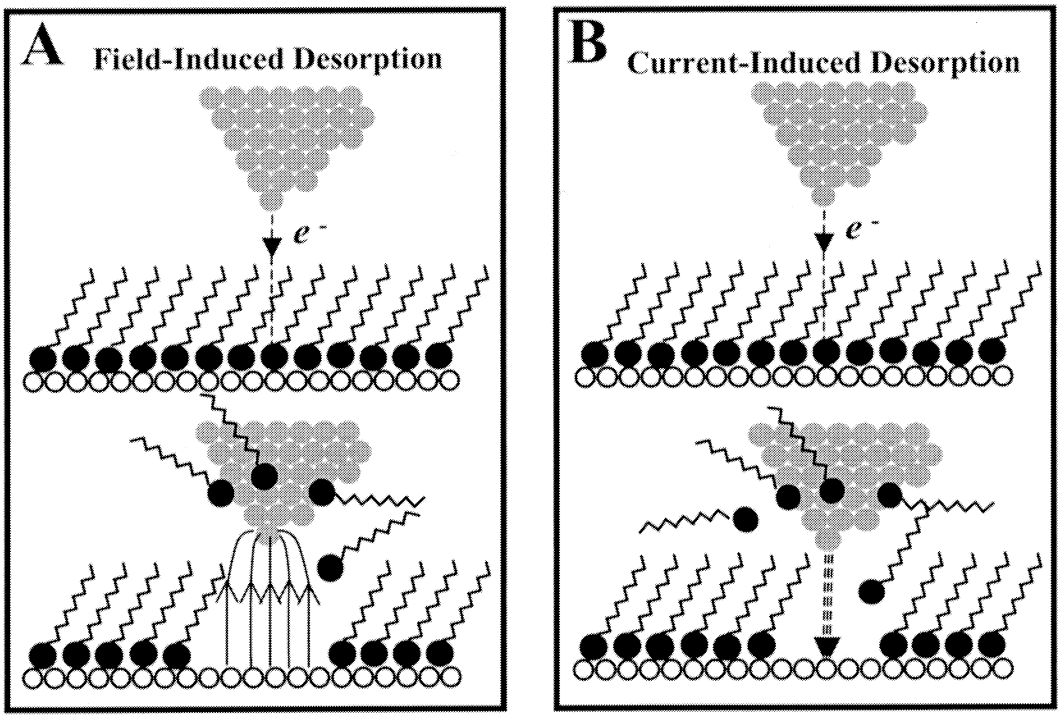

Figure1: Schematic diagrams of two STM-based lithography mechanisms using the electric field (A) and tunneling electrons (B). The imaging and fabrication modes are depicted in the top and bottom rows, respectively.

3.1.1 Field-induced desorption

To measure the strength of applied electric field between the tip and the surface, the STM tip-SAM temini contact point must be precisely determined. This positioning is achieved by first taking the current-distance (I-Z) curve, as shown in Figure 2A. Prior to the tip-SAM surface contact, lnI-Z increases linearly as the tip approaches the surface. The tunneling barrier height Φ can be calculated using

$$\Phi = -0.952[\Delta \ln(I)/ \Delta Z]^2 \quad (1)$$

where I is the tunneling current and Z is the tip-surface separation.[45,46] After contact, the tunneling current continues to increase linearly, with a larger slope, as the tip penetrates into the SAM. The first turning point (indicated in Figure 2A) defines the tip-methyl group contact position, at which I-V curves are acquired, as shown in Figure 2B. I-V curves taken in this manner most accurately reflect the electronic characteristics of tip-SAMs in a junction. Figure 2B shows a typical I-V curve of a decanethiol SAM at contact, for a voltage range of –2.5 to +2.5 V. The curve was acquired as the voltage was swept from a negative sample bias to a positive one. The I-V curve shows that the current was nearly symmetric and linear at very low voltage, and increased exponentially at higher voltages. Two important observations from the I-V

measurements are: (1) at about 2.4 V or beyond (sample positive), a peak occurs, corresponding to a negative differential resistance (dV/dI < 0, or NDR); (2) the I-V profile is not completely symmetric at large voltages. Although the I-V curve can be acquired down to –10 V negative sample bias, it is difficult to get stable I-V measurements beyond +2.5 V due to the occurrence of current spikes.

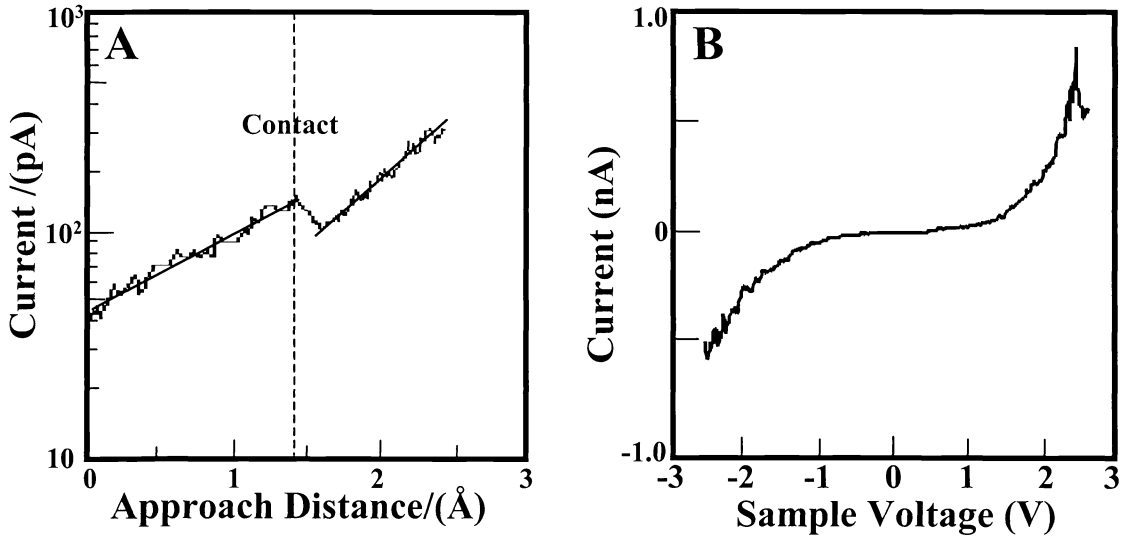

Figure 2: Scanning tunneling spectroscopy of decanethiol SAMs on Au(111). (A) A typical current-distance curve of decanethiol SAMs measured from the setpoint (I = 50 pA and V = 1.0 V). The contact between the tip and the monolayer surface is defined as the first kink point on the lnI-Z curve, indicated by the dash line. (B) I-V characteristic of decanethiol SAMs when the tip is at contact with the SAM surface. At 2.4 V (sample positive), a transition occurs with negative differential resistance (NDR).

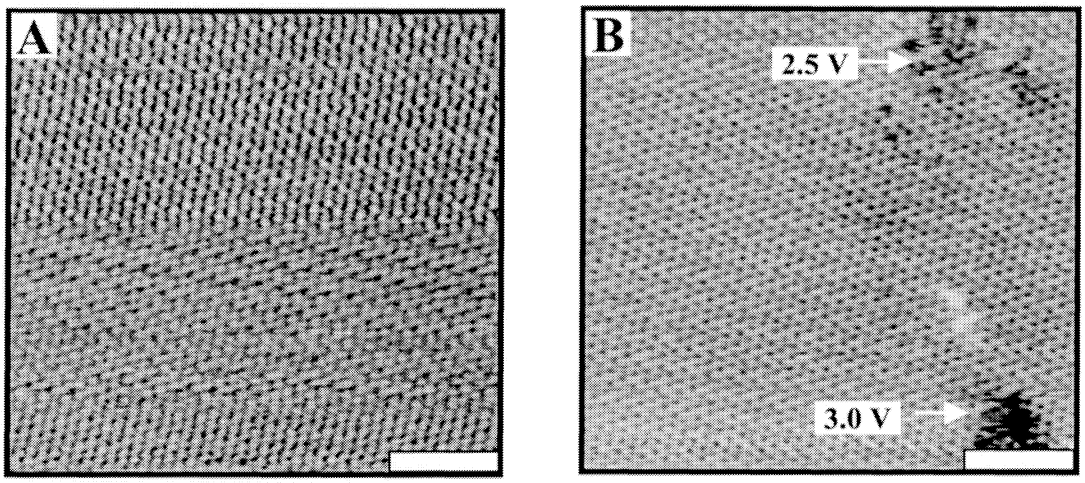

Figure 3: STM-based nanofabrication by field-induced desorption. (A) STM topograph of the decanethiol monolayer taken before applying the threshold field. (B) STM image acquired after fabrication. At 2.5 V, few molecular vacancies are created. At 3.0 V, a hole of 3 nm in diameter is produced. Both scale bars are 4 nm.

In previous studies, observations of NDR for SAM-based junctions have been attributed to tip-molecular interactions or resonant tunneling, i.e. narrow features in the local density of states of the tip apex with the surface.[47,48] The breakdown voltage of SAMs was attributed to an electronic process, although the mechanism was not known.[49-51] To verify and explore the mechanism of the breakdown voltage, we have imaged thiols before, during and after I-V measurements. Molecular resolution STM topographs reveal that the surface of decanethiol SAMs undergoes little change below +2.5 V, as shown in Figure 3A. By increasing the voltage to + 2.5 V, dark holes were generated, as shown in Figure 3B. The depth of these holes is 7 Å, indicating desorption of decanethiol molecules. At a higher voltage of 3.0 V, a larger hole of

3 nm in diameter is produced, corresponding to the removal of about 32 decanethiol molecules. Most of the removed molecules attached to the STM tips, since we observed that continuous scanning will heal the holes, and that materials from the STM tips readsorb onto designated areas with voltage pulsing. Therefore, we conclude that NDR is caused by a local heal the holes, and that materials from the STM tips readsorb onto designated areas with voltage pulsing. Therefore, we conclude that NDR or the breakdown are caused by a local structural change, for example, desorption of the decanethiol molecules under the tip, instead of unknown electronic transitions. This mechanism can be used to produce nanostructures within SAMs.

The observation of a breakdown voltage (+ 2.5 V) may be rationalized by the mechanism of field-induced dissociation and desorption.[31,52-56] From a qualitative perspective, breakdown only occurs at sufficiently large positive bias, not at the reversed polarity, which indicates that it is the effect of an electric field. The electric field measured at the point of breakdown is ~1.8×10^9 V/m, for decanethiol SAMs with a thickness of 1.34 nm. Additional evidence was collected by investigation of the threshold voltage as a function of chain length, or the number of carbons in alkanethiol SAMs. A linear relationship is found between the electric field as a function of the number of carbons. The slope of the line corresponds to a field strength of 1.9×10^9 V/m, which is similar in magnitude to the breakdown electric fields observed by Wold *et al.* in conductive AFM studies,[51] and by Hagg *et al.* in electric breakdown measurements[49] for Hg/SAM/Ag junctions. In thiol SAMs, the partial negative charge for sulfur has been calculated to be ~$0.4e^-$.[57] The S-Au separation is 2.2 Å. The S-Au dipole moment μ is approximately 8.4×10^{-30} C·m (or 2.5 Debye).[58] For a positive bias, the S-Au bond is weakened because the electrical field forces the charge to redistribute, i.e. reduction of the partial charges on S and Au atoms. If the electric field is sufficiently large, the dissociation of S-Au bonds would occur. Analogous observations have been found in the dissociation of Si-NO bonds under a threshold electric field of ~1.2×10^9 V/m.[56] Using *ab initio* density functional cluster theory, the charge redistribution is predicted to occur under high positive local field, which breaks chemical bonds.[55] Since the electrical field is local, up to molecular precision can be achieved in surface fabrication. The newly produced nanostructures can also be characterized and modified in situ.

3.1.2 Current-induced desorption

In comparison to the field-induced mechanism, nanofabrication using tunneling current is shown in Figure 4. First, the SAMs are imaged at 1 V and 10-20 pA to select a fabrication location (Figure 4A). While keeping the voltage constant and the feedback active, the tunneling current is gradually increased by moving the tip towards the surface. The I-Z curve follows an exponential relationship as dictated in quantum tunneling processes until the current reaches the fabrication threshold, at which a large fluctuation of current is observed.[35] The fluctuation is attributed to movements of atoms and molecules within the tunneling junction, e.g. the desorption of thiol molecules. At 200 pA, holes as small as 1 nm in diameter can be produced at 1 V. At a higher tunneling current of 300 pA, a 3 nm hole was produced, as is shown in Figure 4B. The corresponding cursor profiles reveal the depth of the holes to be 0.7 ± 0.2 nm. This observed apparent depth is greater than a single Au(111) step (0.24 nm), but smaller than the thickness of decanethiol SAMs (1.34 nm). This observation is consistent with previous STM studies and with the fact that alkyl chains do not make a significant contribution to the tunneling current. The electronic density of states of hydrocarbon chains is sufficiently distant from the Fermi levels of the tungsten tip and the gold substrate. With the presence of clean W or Pt-Rh tips, the thiols loosely bonded to the gold surface could attach to the tips.

Tunneling current induced desorption can be understood by the following contributions. First, the local electric field causes the redistribution of charges at S-Au bonds. Since the corresponding electric field is estimated to be ~8×10^9 V/m, smaller than the threshold field strength of 1.9×10^9 V/m, the charge redistribution weakens the S-Au bonds, but is not sufficient for bond dissociation. The contribution from the field is supported by our observation that a positive bias is required. At negative sample voltages of –1 to –4 V, no observable desorption was evident, even at 1 nA. The second contribution is from the tunneling current. Tunneling electrons are known to cause the dissociation of chemical bonds. A proposed model is the vibrational excitation of adsorbate molecules by resonant inelastic electron tunneling.[34,59,60] With the weakening of S-Au bonds by local fields, a tunneling current as low as 70 pA can induce decanethiol desorption at a voltage of 2.0 V.

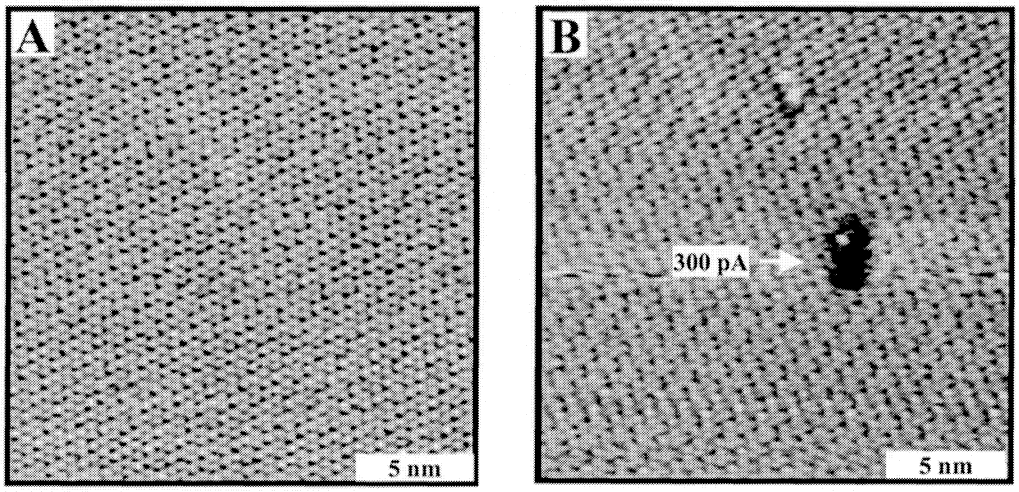

Figure 4: Current-induced desorption by STM. Images of a decanethiol SAM were taken before (A) and after (B) fabrication. A 1 nm hole was fabricated at +1.0 V and 200 pA, and a hole of 3 nm formed at 300 pA

3.2 AFM-based lithography

The methods of our AFM-based lithography are illustrated in Figure 5. First, the surface structure is characterized under a low force or load. Fabrication locations are normally selected in regions with flat surface morphology, e.g., Au(111) plateau areas. The second step is patterning SAMs under high force. In nanoshaving (Figure 6A, bottom), the AFM tip exerts a high local pressure at the contact. This pressure results in a high shear force during the scan, which causes the displacement of SAM adsorbates. During nanoshaving,[35] adsorbate molecules are displaced by an AFM tip during the scan at a load higher than the displacement threshold. Holes and trenches can be fabricated.

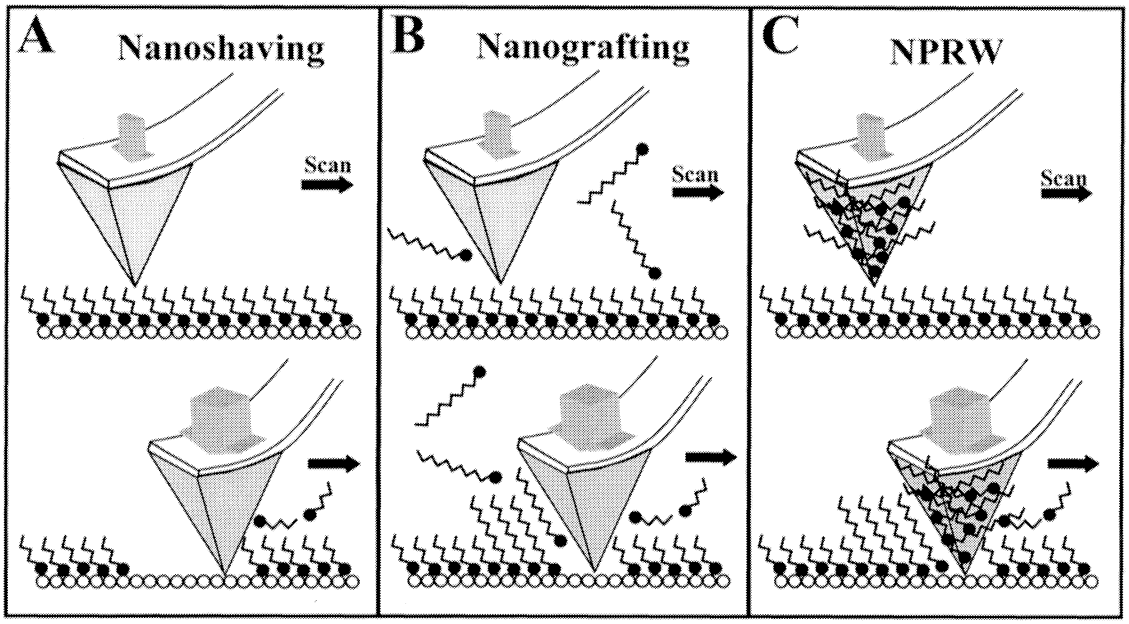

Figure 5: Schematic diagrams of three AFM-based lithography mechanisms using the local pressure exerted by the tip. The imaging and fabrication modes are depicted in the top and bottom rows, respectively.

In nanografting (Figure 5B),[35,44,61] AFM tips are also used to shave thiol molecules from their adsorption sites. The SAM and the AFM cantilever are immersed in a solution containing a different thiol. The thiol molecules in the solution

adsorb on the newly exposed gold surface as the AFM tip plows through the matrix SAM. The nanostructures can be characterized in the third step at reduced loads.

The third AFM-based lithography technique, nanopen reader and writer (NPRW),[62] is developed to fabricate SAMs under ambient conditions. As shown in Figure 5C, a thiol SAM on gold is used as the resist, while an AFM tip is used as a shaver to displace thiols from desired locations under a high force (e.g., 5-10 nN). The tip is precoated with a different adsorbate, normally another thiol. As the tip displaces the matrix molecules, new thiols on the tip adsorb onto the freshly exposed gold substrate following the shaving track of the tip. The resulting patterns can then be characterized under a reduced load (0.05-5 nN).

3.2.1 Nanoshaving

There are a number of requirements to produce sharp nanopatterns using nanoshaving: local displacement, immediate removal of the displaced adsorbate, and absence of readsorption. The fate of the displaced molecules depends on the structure of SAMs and the fabrication environment. Alkanethiols form an ordered structure on Au(111) without cross-linking among nearest neighbors. In air or water, where thiols exhibit little solubility, most of the displaced molecules often remain weakly attached to the gold substrate or SAMs in nearby locations. Therefore, the displacement is mostly reversible and cannot be used to pattern thiol SAMs. Using solvents in which thiols exhibit sufficient solubility such as ethanol or 2-butanol, sharp patterns can be produced. Figure 6A shows a 50 × 60 nm^2 rectangular hole within a $C_{18}S$/Au(111) layer produced in 2-butanol.

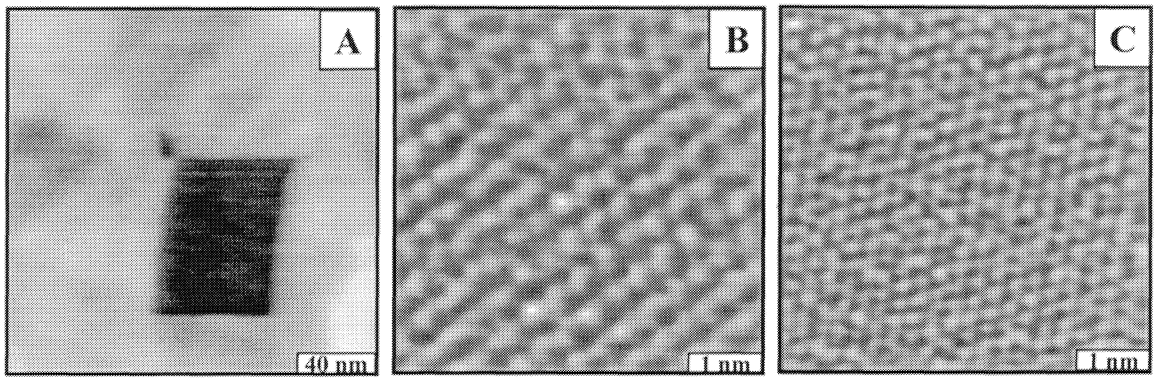

Figure 6: Nanashaving by AFM. (A) 200 × 200 nm^2 topographic images of $C_{18}S$/Au(111) with the thiols shaved away from the central 50 × 60 nm^2 square. (B) A Topographic image (5 × 5 nm^2) of $C_{18}S$/Au(111) was taken in 2-butanol at a load of 1 nN. (C) At a load of 10 nN, periodicity in images B changed into the periodicity of Au(111).

Fabrication force is the key parameters in maintaining a local tip-surface interaction. Extremely high forces in AFM can cause plastic deformation or displacement of the underlying gold substrate. On the other hand, if the force is too low, molecules cannot be displaced completely in one scan. Multiple scans could result in winding edges due to the drift between scans. Since the fabrication threshold varies with the geometry of AFM tips, the structure of the matrix SAMs, and the fabrication environment, the threshold should be determined in situ for each individual experiment before attempting fabrication. The force threshold can be determined by monitoring the changes in surface structure as a function of increasing load. The structural changes are best monitored from molecular resolution images taken at relatively small scanning areas (typically, 3 × 3 to 25 × 25 nm^2). Under low imaging forces, topographic images reveal the molecular packing within SAMs. Figure 6B shows an ordered and closely packed octadecanethiol monolayer on gold. As the load increases, the image remains unchanged at first and then become increasingly distorted at higher forces. A continuous increasing of the imaging force results in a transition in the AFM image from the lattice of SAM to that of the substrate. Figure 6C reveals that the Au(111) substrate have a hexagonal symmetry with a periodicity of 2.88 Å. The load at which the transition occurs is referred to as the displacement threshold. The threshold force is 9.5 nN, which correspond to a local pressure of 0.4 Gpa, assuming the Hertzian contact.

The highest resolution AFM images of thiol SAMs were acquired in liquid media under very low imaging forces (e.g., 0.05 nN).[36,37] The pressure exerted by the tip was ~0.01 GPa (assuming a tip radius of ~100 Å). The van der Waals energy per CH_2 group is ~ 1.5 kcal/mol. Therefore, under such imaging pressure, the AFM tip was in contact with the

methyl temini, which causes only minute local deformations. Increasing the local pressure would increase the deformation, disrupt the packing, and eventually displace thiol molecules from their adsorption sites because the Au-S bond is the weakest at the interface (the binding energies for S-Au, C-C, C-H, and C-S are 40, 145, 81, and 171 kcal/mol, respectively). Increasing the load further would cause the underlying gold substrate to deform.[63]

3.2.2 Nanografting

It is important to point out that the newly nanografted thiol nanostructures not only have an ordered and closely-packed ($\sqrt{3}\times\sqrt{3}$)R30° lattice, but also have fewer defects such as pinholes or uncovered areas.[35,44] The absence of pinhole defects is critical for a faithful pattern transfer when patterned SAMs are used as masks. Using the nanografting procedure, thiols with various chain lengths have been successfully patterned. The observed heights and high-resolution images of these nanostructures indicate that the thiols are close-packed within the patterns. In addition, nanostructures terminated with various functional groups, such as -OH, $-CO_2H$, $-NH_2$, and -CHO have also been produced.[44,64] Compared with other methods for microfabrication, nanografting allows a more precise control over the size and geometry of patterned features and their locations on surfaces. Feature sizes as small as 2×4 nm^2 islands (32 alkanethiol molecules) and 10-nm-wide lines have been fabricated.[35,44,61]

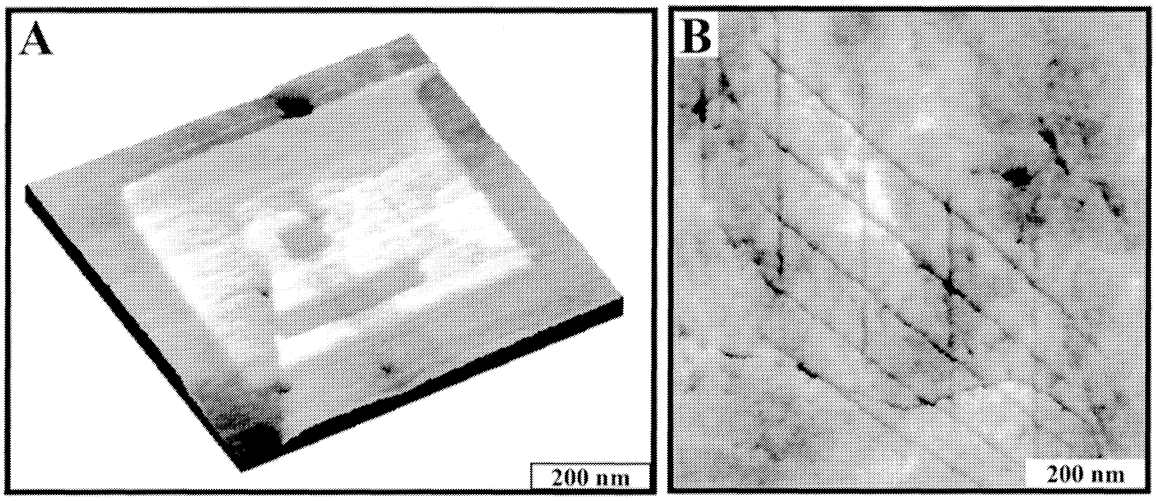

Figure 7: Nanografting by AFM. (A) Fabrication of multicomponent patterns using nanografting. The dimensions of the $C_{18}S$ and $C_{10}CHO$ square patterns, the $C_{10}CHO$ line structure in a $C_{10}S$ matrix are 500×500, 60×60, and 60×300 nm^2, respectively. (D) A 4×4 line structure. Each $C_{11}OH$ line is 10 nm in width within a $C_{18}S$ matrix.

Nanografting can create both positive and negative patterns, depending upon the relative chain length between the new and matrix adsorbates.[35] By changing thiol solution above the matrix layer before each nanografting experiment, we were able to produce multiple nanopatterns with desired arrangements and compositions of thiols. Figure 7A shows three patterns of different heights. First, a rectangular $C_{18}S$ pattern (500×500 nm^2) was nanografted within a $C_{10}S$ matrix SAM. The solution was then replaced with a 0.2 mM $C_{10}CHO$ solution, and then a square pattern (60×60 nm^2) and a line structure of $C_{10}CHO$ was nanofabricated on the top of the $C_{18}S$ island. The $C_{18}S$ and $C_{10}CHO$ patterns were 0.8 ± 0.1 and 0.2 ± 0.1 nm taller than the surrounding $C_{10}S$ matrix, respectively. In Figure 7B, a 4×4 $C_{11}OH$ line structure was fabricated within a $C_{18}S$ monolayer. Each line is 10 nm wide. Molecular resolution images of the nanoislands revealed a hexagonal lattice with a lattice constant of 0.50 nm. Together, the height measurements and molecular resolution images indicated that the chains were closely packed within the nanoislands. The ability to produce multiple patterns from different adsorbates satisfies a basic requirement for fabrication of various nanoelectronic devices and sensor arrays.

The unique advantage of nanografting is its ability to systematically change the patterns in situ without restarting of the entire fabrication process. In Figure 8, two parallel $C_{18}S$ nanolines (10×50 nm^2) were first produced in a $C_{10}S$ matrix with a separation of 20 nm. The interline separation was then increased to 65 nm. To perform this operation, we erased the right line by scanning the area defining this line at a high force in a $C_{10}SH$ solution. After the line on the right was erased, we then replaced the $C_{10}SH$ solution with a $C_{18}SH$ solution and fabricated a new line further to the right of the

first $C_{18}S$ line, thereby increasing the interline spacing to 65 nm. In contrast to other microfabrication methods, the use of nanografting to modify a prepared pattern does not require the generation of new masks or a repeat of an entire fabrication process. This ability to interactively pattern on the nanometer scale provides a unique opportunity for studying size-dependent properties systematically and unambiguously as all other experimental conditions can be held constant.

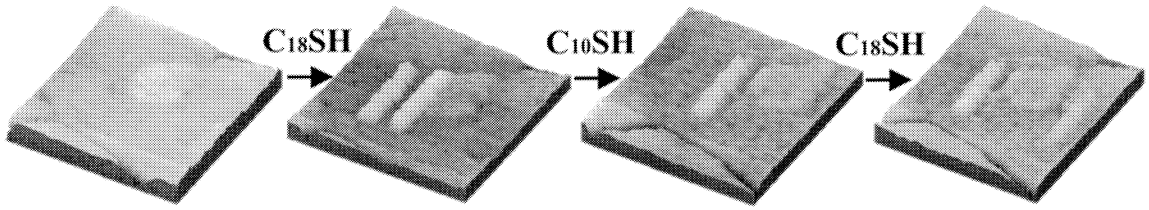

Figure 8: In situ modification of the grafted nanostructures. (A) AFM image of the matrix $C_{10}S$ SAM before fabrication. (B) After fabrication of two parallel $C_{18}S$ nanolines with dimensions of 10×50 nm^2 and a separation of 20 nm. (C) Erasure of the right line by scanning its area under a high imaging force in a $C_{10}SH$ solution. (D) Refabrication of the second line by scanning under a high imaging force in $C_{18}SH$ solution. The interline spacing was increased to 65 nm. The spatial precision for this fabrication is 2 nm.

3.2.2 Nanopen reader and writer (NPRW)

Nanostructures of various thiols can be produced under ambient laboratory conditions by NPRW.[62] In the examples shown in Figure 9, the resist was a $CH_3(CH_2)_9S$/Au(111) SAM. The tip, made of Si_3N_4 with a force constant of 0.1 N/m was first coated with $CH_3(CH_2)_{17}SH(C_{18}SH)$ by soaking in a saturated $C_{18}SH$ (2-butanol) solution for 15 min and then allowed to dry under a gentle flux of N_2 for 30 min. Within the 200×200 nm^2 pattern of $C_{18}S$ shown in Figure 10A, three single atomic Au(111) steps are clearly visible. The $C_{18}S$ pattern is 8.3 Å higher than the surrounding $C_{10}S$ monolayer and thus appears brighter in the topographic image shown in Figure 9A. Zooming into any areas within the pattern or matrix, the $(\sqrt{3}\times\sqrt{3})R30°$ periodicity can be resolved (see Figure 9B). Together the height and periodicity measurements compare well with the known structure of alkanethiol SAMs. The coated tip lasted throughout the experiment (more than 5 h) without becoming dull or running out of ink. Figure 9C demonstrate the fabrication of a nanoarray, which contains 80×80 nm^2 square islands of $C_{18}S$ within a double layer of $C_{15}COOH$. The spacing between C_{18} islands is 80 nm apart. In addition to alkanethiol nanopatterns, NPRW has been used to produce nanostructures with various functionalities including -CHO, -COOH, -SH, -OH, etc., which demonstrates the generality of this approach and provides opportunities to build complex architectures using these patterns.

Similar to nanografting, the spatial precision of NPRW is determined by the intrinsic stability of the AFM and the tip-substrate contact area during fabrication. The tip-substrate contact depends on the force exerted during fabrication and the sharpness of the tip. The resolution of NPRW is independent of the texture of the paper and the humidity of the environment. In addition, NPRW is easier to perform and expands the medium of nanografting from solution phase to both solution and ambient environments. In nanografting, fresh solvent must be injected after fabrication to prevent exchange reactions, whereas with NPRW, the exchange reaction is effectively prevented because the imaging medium does not contain adsorbate molecules.

The thiols within the patterns are ordered and closely packed as shown in the high-resolution images in Figure 9. These nanostructures have a very low density of defects and no observable impurities. In addition, the self-assembly occurs following a very fast kinetics (faster than the scanning speed of 40 ms per line). Following the example of our systematic study in nanografting experiments, these observations are attributed to the change in reaction pathway due to a spatially confined microenvironment, i.e., the newly exposed gold surface is confined by the AFM tip and the surrounding thiols.[37] Since thiols are located on the tip, the adsorption is further accelerated because the reactant is delivered to the surface by the tip. As a result of the spatial constraint and the high local density of thiols, the self-assembly process in NPRW follows a pathway similar to nanografting, which differs from the unconstrained self-assembly. The fast kinetics in NPRW allows fast fabrication and the use of a wide range of scanning speeds because the adsorption process is faster than the scan.

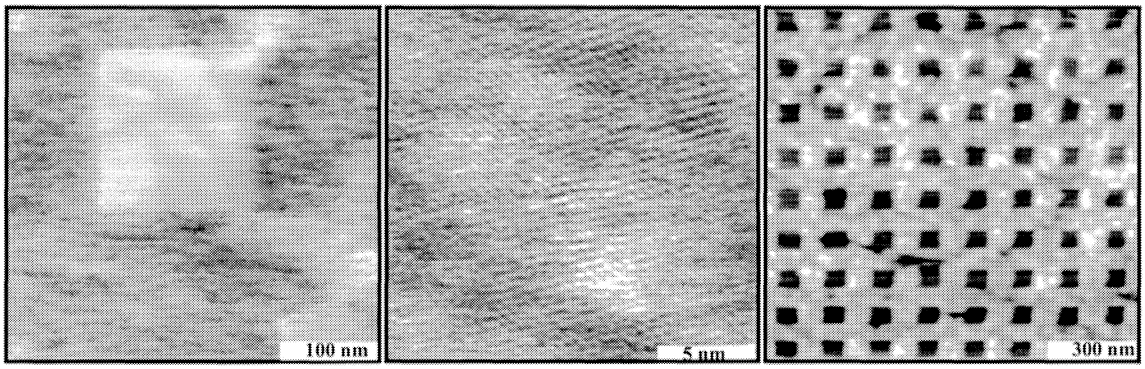

Figure 9: Nanopen reader and writer (NPRW) by AFM. (A) a 400 × 400 nm^2 topographic image of $C_{10}S$/Au SAM containing a 200 × 200 nm^2 square of a $C_{18}S$ pattern; (B) a high-resolution 20 × 20 nm^2 image of the matrix $C_{10}S$ as indicated in (A); (C) a 1200 × 1200 nm^2 topographic image of a 8 × 9 $C_{15}COOH$ nanostructures (80 × 80 nm^2) in $C_{18}S$. The spacing between C_{18} islands is 80 nm.

The image contrast in NPRW experiments is sharper than similar images acquired without coating the tips. This observation is contrary to the speculation that a coated tip may compromise the AFM resolution because the tip becomes duller and more hairy than the corresponding uncoated tip. Etch pits, single atomic Au(111) steps, and the periodicity of the thiol lattices can be observed routinely in air (Figure 9B). In Figure 9B, the periodicity and domain boundaries were both visible in a relatively large scan, 20 × 20 nm^2. The improved resolution may be attributed to a strong tip-surface interaction as a result of coating tips with the functionality similar to the surface. Such strong interactions enhance the surface corrugation of the SAMs detected by the AFM tip, and thus sharpen the image contrast. As demonstrated in this and our previous studies,[44,61] AFM can reach true molecular resolution. High-resolution AFM images of these nanopatterns show no presence of impurities. We attribute this observation to the high local concentration of thiols on the tip and the fact that matrix thiols were displaced and removed from the adsorption sites efficiently during the fabrication process.

4. CONCLUSIONS

We have developed several SPL-based methods to produce nanometer-sized patterns within SAMs. The key to achieving high spatial precision is to keep the tip-surface interactions strong and local. In this work, we introduced three AFM-based methods, nanoshaving, nanografting, and NPRW, which rely on the local force, and two STM-based techniques, field-induced desorption and electron-induced desorption, which use the local field and tunneling electrons for fabrication. Compared with other techniques used to fabricate microstructures of SAMs, SPL, especially STM-based lithography, offers the highest spatial precision. While our STM lithography is carried out in UHV, the AFM fabrication can be done in an ambient and liquid environment and is relatively simple to set up. Edge resolution of several nanometers is routinely obtained, and molecular precision can be achieved with an ultrasharp tip. The fabricated nanostructures can be characterized with molecular resolution in situ using the same tip. Using nanografting, one can also quickly change and/or modify the fabricated patterns in situ without changing the mask or repeating the entire fabrication procedure. Various examples discussed in this study demonstrate that SPL can be used as a generic method for nanofabrication of SAMs. In addition, the SPL process itself allows many new phenomena to be revealed and studied, such as spatially confined reactions.[37] In combination with protein immobilization techniques, we used SPL to produce nanometer-sized protein patterns.[12,64]

A well-known limitation of all SPL procedures is that the fabrication steps are serial instead of parallel in nature, which results in a relatively low fabrication speed. Therefore, at present, SPL is used as a research tool in laboratories instead of as a manufacturing tool for high-throughput applications. In addition, more pattern-transfer protocols such as selective etching and deposition also need to be tested to explore the feasibility of using SPL to produce nanostructures of metals and semiconductors. Furthermore, the ability to change nanostructures in situ provides a unique opportunity for systematic studies of size-dependent properties of nanostructures in the near future. Attempts to improve fabrication throughput include using tip arrays and making the lithographic process automatic.

The strength of our approach is the ability to engineer and image complex molecular architectures with high spatial precision. The precisely engineered nanostructures allow for the exploration of chemical and biochemical reactions under spatially well-defined and controlled environments. Although not yet practical for high-throughput applications and manufacturing, SPL studies provide fundamental information on tip-surface interactions, structures, and properties on a nanoscopic level. These studies shall serve as a useful guide in the nanofabrication of nanoelectronic devices, biosensors, and biochips.

Acknowledgments

We appreciate many helpful discussions with Jayne Garno, Vladimir Komanicky and Maozi Liu at UC Davis. This work is supported by the University of California, Davis, and NSF (CHE-0244830, and Stanford University-CPIMA program).

References

1. J. M Tour, "Molecular electronics. Synthesis and testing of components", *Accounts of Chemical Research,* **33**, 791, 804, 2000.

2. C. Joachim, J. K. Gimzewski, A. Aviram, "Electronics using hybrid-molecular and mono-molecular devices". *Nature,***408**, 541-548, 2000.

3. M. P. de Boer, T. M. Mayer, "Tribology of MEMS", *Mrs Bulletin,* **26**, 302-304, 2001.

4. R. Maboudian, W. R. Ashurst, C. Carraro, "Tribological challenges in micromechanical systems", *Tribology Letters,* **12**, 95-100, 2002.

5. K. Komvopoulos, W. Yan, "A fractal analysis of stiction in microelectromechanical systems", *Journal of Tribology-Transactions of the Asme,* **119**, 391-400, 1997.

6. R. M. Crooks, A. J. Ricco, "New organic materials suitable for use in chemical sensor arrays", *Accounts of Chemical Research,* **31**, 219-227, 1998.

7. S. Flink, F. van Veggel, D. N. Reinhoudt, "Sensor functionalities in self-assembled monolayers", *Advanced Materials,* **12**, 1315-1328, 2000.

8. A. .R Bishop, R. G. Nuzzo, " Self-assembled monolayers: Recent developments and applications", *Current Opinion in Colloid & Interface Science,* **1**, 127-136, 1996.

9. I. Willner, E. Katz, "Integration of layered redox proteins and conductive supports for bioelectronic applications", *Angewandte Chemie-International Edition,* **39**, 1180-1218, 2000.

10. M. Mrksich, et al., "Controlling cell attachment on contoured surfaces with self-assembled monolayers of alkanethiolates on gold", *Proceedings of the National Academy of Sciences of the United States of America,* **93**, 10775-10778, 1996.

11. L. Deng, M. Mrksich, G. M. Whitesides, " Self-assembled monolayers of alkanethiolates presenting tri(propylene sulfoxide) groups resist the adsorption of protein", *Journal of the American Chemical Society,* **118**, 5136-5137, 1996.

12. G. Y. Liu, N. A. Amro, " Positioning protein molecules on surfaces: A nanoengineering approach to supramolecular chemistry", *Proceedings of the National Academy of Sciences of the United States of America,* **99**, 5165-5170, 2002.

13. K. Wadu-Mesthrige, N. A. Amro, J. C. Garno, S. Xu, G. Y. Liu, "Fabrication of nanometer-sized protein patterns using atomic force microscopy and selective immobilization", *Biophysical Journal,* **80**, 1891-1899, 2001.

14. J. Y. Huang, D. A. Dahlgren, J. C. Hemminger, "Photopatterning of Self-Assembled Alkanethiolate Monolayers on Gold - a Simple Monolayer Photoresist Utilizing Aqueous Chemistry" *Langmuir,* **10**, 626-628, 1994.

15. M. J. Tarlov, D. R. F. Burgess, G. Gillen, G. "Uv Photopatterning of Alkanethiolate Monolayers Self-Assembled on Gold and Silver", *Journal of the American Chemical Society,* **115**, 5305-5306, 1993.

16. Y. N. Xia, G. M. Whitesides, "Soft lithography", *Annual Review of Materials Science,* **28**, 153-184, 1998.

17. N. L. Abbott, A. Kumar, G. M.Whitesides, "Using Micromachining, Molecular Self-Assembly, and Wet Etching to Fabricate 0.1-1-Mu-M-Scale Structures of Gold and Silicon", *Chemistry of Materials,* **6**, 596-602, 1994.

18. A. Kumar, N. L. Abbott, E. Kim, H. A. Biebuyck, G. M. Whitesides, "Patterned Self-Assembled Monolayers and Mesoscale Phenomena", *Accounts of Chemical Research,* **28**, 219-226, 1995.

19. Y. N. Xia, G. M. Whitesides, "Use of Controlled Reactive Spreading of Liquid Alkanethiol on the Surface of Gold to Modify the Size of Features Produced by Microcontact Printing", *Journal of the American Chemical Society,* **117**, 3274-3275, 1995.

20. J. A. M. Sondaghuethorst, H. R. J. Vanhelleputte, L. G. J. Fokkink, "Generation of Electrochemically Deposited Metal Patterns by Means of Electron-Beam (Nano)Lithography of Self-Assembled Monolayer Resists" *Applied Physics Letters,* **64**, 285-287, 1994.

21. K. K. Berggren, et al., "Microlithography by Using Neutral Metastable Atoms and Self-Assembled Monolayers", *Science,* **269**, 1255-1257, 1995.

22. D. A. Offord, C. M. John, M. R. Linford, J. H. Griffin, "Contact-Angle Goniometry, Ellipsometry, and Time-of-Flight Secondary-Ion Mass-Spectrometry of Gold Supported, Mixed Self-Assembled Monolayers Formed from Alkyl Mercaptans", *Langmuir,* **10**, 883-889, 1994.

23. K. Tamada, M. Hara, H. Sasabe, W. Knoll, "Surface phase behavior of n-alkanethiol self-assembled monolayers adsorbed on Au(111): An atomic force microscope study", *Langmuir,* **13**, 1558-1566, 1997.

24. W. A. Hayes, H. Kim, X. H. Yue, S. S. Perry, C. Shannon, "Nanometer-scale patterning of surfaces using self-assembly chemistry .2. Preparation, characterization, and electrochemical behavior of two-component organothiol monolayers on gold surfaces", *Langmuir,* **13**, 2511-2518, 1997.

25. G. Binning, H. Rohrer, C. Gerber, E. Weibel, "Surface Studies by Scanning Tunneling Microscopy", *Physical Review Letters,* **49**, 57-61, 1982.

26. G. Binnig, C. F. Quate, C. Gerber, "Atomic Force Microscope", *Physical Review Letters,* **56**, 930-933, 1986.

27. D. M. Eigler, E. K. Schweizer, "Positioning Single Atoms with a Scanning Tunneling Microscope", *Nature,* **344**, 524-526, 1990.

28. M. F. Crommie, C. P. Lutz, D. M. Eigler, "Confinement of Electrons to Quantum Corrals on a Metal-Surface", *Science,* **262**, 218-220, 1993.

29. T. A. Jung, R. R. Schlittler, J. K. Gimzewski, H. Tang, C. Joachim, "Controlled room-temperature positioning of individual molecules: Molecular flexure and motion", *Science,* **271**, 181-184, 1996.

30. P. Avouris, "Manipulation of Matter at the Atomic and Molecular-Levels", *Accounts of Chemical Research,* **28**, 95-102, 1995.

31. L. W. Lyo, P. Avouris, "Field-Induced Nanometer-Scale to Atomic-Scale Manipulation of Silicon Surfaces with the Stm", *Science,* **253**, 173-176, 1991.

32. C. T. Salling, M. G. Lagally, "Fabrication of Atomic-Scale Structures on Si(001) Surfaces", *Science,* **265**, 502-506, 1994.

33. R. M. Nyffenegger, R. M. Penner, "Nanometer-scale surface modification using the scanning probe microscope: Progress since 1991", *Chemical Reviews,* **97**, 1195-1230, 1997.

34. W. Ho, "Inducing and viewing bond selected chemistry with tunneling electrons" *Accounts of Chemical Research,* **31**, 567-573, 1998.

35. G. Y. Liu, S. Xu, Y. L. Qian, "Nanofabrication of self-assembled monolayers using scanning probe lithography", *Accounts of Chemical Research,* **33**, 457-466, 2000.

36. H. J. Butt, K. Seifert, E. Bamberg, "Imaging Molecular Defects in Alkanethiol Monolayers with an Atomic-Force Microscope", *Journal of Physical Chemistry,* **97**, 7316-7320, 1993.

37. S. Xu, P. E. Laibinis, G. Y. Liu, "Accelerating the kinetics of thiol self-assembly on gold - A spatial confinement effect", *Journal of the American Chemical Society,* **120**, 9356-9361, 1998.

38. G. E. Poirier, "Characterization of organosulfur molecular monolayers on Au(111) using scanning tunneling microscopy", *Chemical Reviews,* **97**, 1117-1127, 1997.

39. C. A. McDermott, M. T. McDermott, I. B. Green, M. D. Porter, "Structural Origins of the Surface Depressions at Alkanethiolate Monolayers on Au(111) - a Scanning Tunneling and Atomic-Force Microscopic Investigation", *Journal of Physical Chemistry,* **99**, 13257-13267, 1995.

40. E. Delamarche, B. Michel, H. A. Biebuyck, C. Gerber, "Golden interfaces: The surface of self-assembled monolayers", *Advanced Materials,* **8**, 719-726, 1996.

41. W. T. Muller, et al. "A Strategy for the Chemical Synthesis of Nanostructures", *Science,* **268**, 272-273, 1995.

42. R. D. Piner, J. Zhu, F. Xu, S. H. Hong, C. A. Mirkin, ""Dip-pen" nanolithography", *Science,* **283**, 661-663, 1999.

43. C. B. Ross, L. Sun, R. M. Crooks, "Scanning Probe Lithography .1. Scanning Tunneling Microscope Induced Lithography of Self-Assembled N-Alkanethiol Monolayer Resists", *Langmuir,* **9**, 632-636, 1993.

44. S.Xu, S. Miller, P. E. Laibinis, G. Y. Liu, "Fabrication of nanometer scale patterns within self-assembled monolayers by nanografting", *Langmuir,* **15**, 7244-7251, 1999.

45. J. K. Gimzewski, R. Moller, "Transition from the Tunneling Regime to Point Contact Studied Using Scanning Tunneling Microscopy", *Physical Review B,* **36**, 1284-1287, 1987.

46. L. Olesen, et al. "Apparent barrier height in scanning tunneling microscopy revisited", *Physical Review Letters,* **76**, 1485-1488, 1996.

47. Y. Q. Xue, et al. "Negative differential resistance in the scanning-tunneling spectroscopy of organic molecules", *Physical Review B,* **59**, R7852-R7855, 1999.

48. F. R. F. Fan, et al. "Determination of the molecular electrical properties of self- assembled monolayers of compounds of interest in molecular electronics", *Journal of the American Chemical Society,* **123**, 2454-2455, 2001.

49. R. Haag, M. A. Rampi, R. E. Holmlin, G. M. Whitesides, "Electrical breakdown of aliphatic and aromatic self-assembled monolayers used as nanometer-thick organic dielectrics", *Journal of the American Chemical Society,* **121**, 7895-7906, 1999.

50. X. D. Cui, et al. "Making electrical contacts to molecular monolayers", *Nanotechnology,* **13**, 5-14, 2002.

51. D. J. Wold, C. D. Frisbie, "Fabrication and characterization of metal-molecule-metal junctions by conducting probe atomic force microscopy", *Journal of the American Chemical Society,* **123**, 5549-5556, 2001.

52. P. Avouris, I. W. Lyo, "Probing the Chemistry and Manipulating Surfaces at the Atomic Scale with the Stm", *Applied Surface Science,* **60-1**, 426-436, 1992.

53. P. Avouris, et al. "Breaking individual chemical bonds via STM-induced excitations", *Surface Science,* **363**, 368-377, 1996.

54. H. C. Akpati, P. Nordlander, L. Lou, P. Avouris, "The effects of an external electric field on the adatom-surface bond: H and Al adsorbed on Si(111)" *Surface Science,* **372**, 9-20, 1997.

55. H. C. Akpati, P. Nordlander, L. Lou, P. Avouris, "A density-functional study of the effects of an external electric field on admolecule-surface systems", *Surface Science,* **401**, 47-55, 1998.

56. M. A. Rezaei, B. C. Stipe, W. Ho, "Atomically resolved adsorption and scanning tunneling microscope induced desorption on a semiconductor: NO on Si(111)-(7X7)", *Journal of Chemical Physics,* **110**, 4891-4896, 1999.

57. H. Sellers, A. Ulman, Y. Shnidman, J. E. Eilers, "Structure and Binding of Alkanethiolates on Gold and Silver Surfaces - Implications for Self-Assembled Monolayers", *Journal of the American Chemical Society,* **115**, 9389-9401, 1993.

58. R. W. Zehner, B. F. Parsons, R. P. Hsung, L. R. Sita, " Tuning the work function of gold with self-assembled monolayers derived from X- C6H4-C C- (n)C6H4-SH (n = 0, 1, 2; X = H, F, CH3, CF3, and OCH3)", *Langmuir,* **15**, 1121-1127, 1999.

59. B. C. Stipe, et al. "Single-molecule dissociation by tunneling electrons", *Physical Review Letters,* **78**, 4410-4413, 1997.

60. N. Lorente, M. Persson, "Theoretical aspects of tunneling-current-induced bond excitation and breaking at surfaces", *Faraday Discussions*, 277-290, 2000.

61. S. Xu, G. Y. Liu, "Nanometer-scale fabrication by simultaneous nanoshaving and molecular self-assembly" *Langmuir,* **13**, 127-129, 1997.

62. N. A. Amro, S. Xu, G. Y. Liu, "Patterning surfaces using tip-directed displacement and self- assembly", *Langmuir,* **16**, 3006-3009, 2000.

63. R. W. Carpick, M. Salmeron, "Scratching the surface: Fundamental investigations of tribology with atomic force microscopy", *Chemical Reviews,* **97**, 1163-1194, 1997.

64. K. Wadu-Mesthrige, S. Xu, N. A. Amro, G. Y. Liu, "Fabrication and imaging of nanometer-sized protein patterns", *Langmuir,* **15**, 8580-8583, 1999.